Chinese Chemical Letters 36 (2025) 110290

Contents lists available at ScienceDirect

Chinese Chemical Letters

journal homepage: www.elsevier.com/locate/cclet

A near-infrared naphthalocyanine photosensitizer with superior light absorption and renal clearance for type-I photodynamic and photothermal combination therapy

Li Li, Jiale Wen, Xiaojun Zhang, Shuwen Fu, Zixuan Chen, Kai Huang, Luyue Fang, Tinghe Zhao, Peipei Zhang, Xingshu Li*

Fujian Provincial Key Laboratory of Cancer Metastasis Chemoprevention and Chemotherapy, College of Chemistry, Fuzhou University, Fuzhou 350108, China

ARTICLE INFO

Article history:
Received 30 April 2024
Revised 21 July 2024
Accepted 22 July 2024
Available online 23 July 2024

Keywords:
Naphthalocyanine
Near-infrared absorption
Renal clearance
Superoxide anion
Type-I photosensitizer

ABSTRACT

Currently, it is still a challenge to develop an organic photosensitizer (PS) with outstanding near-infrared absorption, low O_2 dependence, precise tumor targeting and rapid clearance through the kidney to improve the overall outcome of phototherapy. In this study, we have designed an organic PS (NcPB) with an excellent near-infrared light absorption through a refined molecular strategy. Meanwhile, NcPB was assembled into nanoparticles with different sizes (NanoNcPB-1 and NanoNcPB-0) by a supramolecular modulation strategy. As the results, the nanoparticle with an ultra-small size (NanoNcPB-1) generated a large number of superoxide anion ($O_2^{\bullet-}$) in a low-O_2-dependent manner and release plenty of heat. Furthermore, the results of *in vivo* experiments demonstrated that NanoNcPB-1 actively accumulated in tumor tissues and showed a 92% tumor inhibition after photodynamic and photothermal combination therapy. More importantly, NanoNcPB-1 could be rapidly cleared from the body of mice *via* the renal pathway, which alleviates potential side effects of prolonged retention of PS in the circulation.

Cancer brings about severe and urgent threats to human beings [1,2]. Unlike conventional treatment modalities, phototherapy is considered a promising strategy for cancer treatment due to its high selectivity, low side effects and non-invasiveness [3]. Photodynamic therapy (PDT) and photothermal therapy (PTT) are two forms of phototherapy that use light-activated photosensitizers (PSs) to produce reactive oxygen species (ROS) or heat that cause cell death [4,5]. In general, the combination treatment of PDT and PTT can compensate for the shortcomings of each therapy and maximize its advantages. For example, in addition to acting as a trigger for the death of cancer cells, the thermal effect of PTT stimulates blood circulation within the tumor, which increases the amount of O_2 delivered to the hypoxic tumor tissues [6-9]. For another, PDT-produced ROS can also enhance PTT efficiency by inhibiting hot shock proteins [10-12].

To date, the type-II mechanism has been adopted for the majority of PDT-related PSs linked to clinical or preclinical applications [13,14]. In this process, singlet oxygen ($^1O_2$) is produced by the PSs in their triplet excited state ($^3PS^*$) transferring energy to the surrounding O_2 [15-17]. The restricted O_2 supply significantly reduces the effectiveness of these PSs for PDT because of the aberrant proliferation of tumor cells [18-22]. Conversely, in the type I mechanism of PDT, ROS are generated through a hydrogen or electron transfer process between $^3PS^*$ and the biological substrate, greatly reducing the degree of O_2 requirement [23-25]. The PSs that undergo the type-I pathway are getting more and more attention [26-28]. However, the absorption wavelength of PSs is mainly focused on the ultraviolet and visible region, which limits their clinical translation due to the poor tissue penetration depth of the light [29,30]. In contrast, the near-infrared (NIR) light has better penetration depth and biocompatibility with the living organisms, minimizing the scattering and attenuation of the irradiation in the tissues [31-34]. Therefore, NIR PS which following the type-I mechanism is beneficial for improving the therapeutic efficiency of PDT and PTT. Furthermore, controlling the ROS oxidation and heat reaction to occur within the target sites is crucial to ensuring the therapeutic outcomes [35,36]. Therefore, it is conceivable that NIR PSs with the ability to target tumor tissues and undergo the type-I pathway could offer more efficacious phototherapy. Currently, report of these perfect agents is scarce.

In this work, we have achieved a strong NIR absorption and active tumor targeting through an ingenious design of phthalocyanine molecule by extending the π-conjugate system and

* Corresponding author.
E-mail address: xingshuli@fzu.edu.cn (X. Li).

https://doi.org/10.1016/j.cclet.2024.110290
1001-8417/

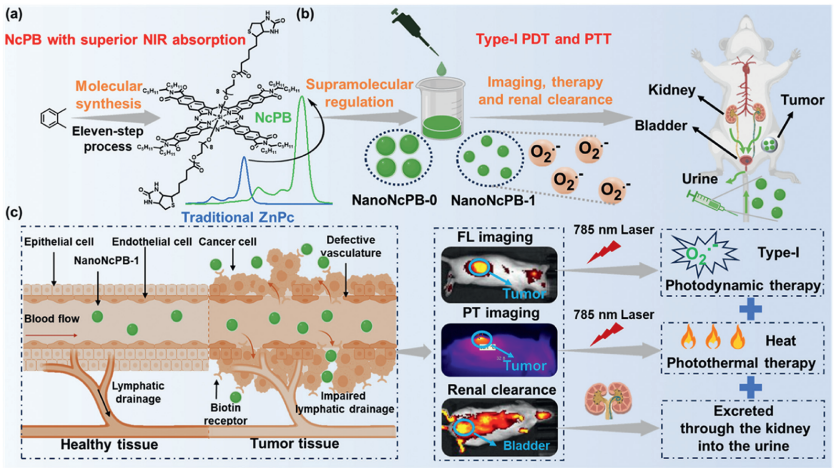

Fig. 1. (a) Schematic representation of the novel naphthalocyanine molecule (NcPB) that has improved optical properties by reducing optical bandgap. (b) Schematic representation of the supramolecular regulation of NcPB to generate nanostructured naphthalocyanine with different sizes. (c) Schematic representation of *in vivo* fluorescence and photothermal imaging, renal clearance pathway and tumor-targeted PDT of NanoNcPB-1. The graph was adapted from https://biorender.com/biorender-templates.

incorporating an actively targeted biotin unit. As can be seen from Fig. 1, the synthesized naphthalocyanine (NcPB) exhibits an excellent light absorption with a molar extinction coefficient of 4.9 ($\times 10^5$ L mol^{-1} cm^{-1}), which is 2.6-fold that of commercial zinc(II) phthalocyanine (ZnPc). More importantly, it is also much higher than currently available small molecule organic dyes [37]. Additionally, NcPB has a significant Q-band absorption at 787 nm, which is red-shifted by 119 nm compared to ZnPc. Interestingly, NcPB can be assembled into nanoparticles with different size by adding surfactants in different ratios. It is found that the nanoparticles (NanoNcPB-1) with ultra-small size demonstrated an effective type-I photoreaction to produce a large amount of superoxide anion ($O_2^{\bullet-}$) and a notable vibrational relaxation to produce a comparatively efficient photothermal conversion, unlike the traditional PSs based on phthalocyanines that undergo a type-II photosensitization. Therefore, this agent combines the action of PDT and PTT, which improves the overall efficacy of phototherapy significantly. Following an intravenous injection, NanoNcPB-1 demonstrated an outstanding tumor accumulation compared to nanoparticles (NanoNcP-1) without biotin-targeting ability. Moreover, NanoNcPB-1 showed a 92% tumor inhibition after combination therapy of PDT and PTT. Excitingly, NanoNcPB-1 can be excreted from the body of mice as raw drugs *via* the renal clearance pathway. As a result, no obvious histopathological abnormality was observed from normal organs by hematoxylin and eosin (H&E) staining, verifying the excellent biocompatibility of NanoNcPB-1.

We selected the silicon phthalocyanine as the main molecular scaffold for the design of novel PSs because of its following advantages: strong absorption, considerable ROS quantum yield, and adaptable photochemical properties. Here, we adopted a conventional strategy by extending the π-conjugated system to achieve NIR absorption. However, the extension of the π-conjugated system leads to some undesirable defects of this dye, such as large hydrophobic structure, poor water solubility, and severe intermolecular aggregation. To address the side effects of the π-extension strategy, we peripherally modified the naphthalocyanine with a lipophilic long alkyl chain to improve its solubility, as well as axially modified the naphthalocyanine with a polyethylene glycol chain to increase its biocompatibility. On the other hand, due to the abnormal growth and proliferation of cancer cells, the demand for biotin in tumor is higher than that in normal tissues, resulting in the expression of biotin receptors in many cancer cells, which makes it a prospective marker for cancer diagnosis and specific therapy [38]. Ultimately, we modified the biotin unit at the end of the polyethylene glycol to improve its ability to target tumor tissues. The naphthalocyanine (NcPB) with the biotin unit was synthesized through an eleven-step process. The naphthalocyanine without biotin units (NcP) was also synthesized as a control. The detailed synthesis scheme and characterization are shown in Figs. S1–S4 (Supporting information).

Firstly, we used an ultraviolet spectrophotometer to investigate the light absorption capacity of NcPB and NcP in *N*,*N*-dimethylformamide (DMF). ZnPc was used as a control because it typically exhibits strong light absorption and photodynamic activity in the optimal phototherapy window. As shown in Fig. 2a, NcPB and NcP exhibit Q-band absorption peaks at 787 nm and 786 nm, respectively. In addition, NcPB and NcP have strong light absorptions, with molar extinction coefficients (ε) of 4.9 and 3.8 ($\times$ 10^5 L mol^{-1} cm^{-1}), respectively. Light-absorbing capacities of NcPB and NcP are 2.6- and 2.0-fold than that of the commercial ZnPc. According to the previous reports, the energy bandgap (E_g) is frequently used to describe the minimum energy required for a substance to be able to absorb a photon and undergo a jump [39,40]. Therefore, we investigated the E_g of NcPB and NcP using cyclic voltammetry in order to determine the cause of the increased light absorption. As shown in Fig. 2b and Table S1 (Supporting information), the E_g of ZnPc, NcP and NcPB were calculated to be 1.15, 1.11 and 1.05 eV, respectively. Based on the above results, we speculate that a smaller E_g is favorable for enhanced light absorption. Therefore, compared with ZnPc, NcPB not only achieved a NIR absorption by extending the π-conjugation system, but also enhanced light-absorption capacity by reducing E_g (Fig. 2c). These superior optical properties should open a new avenue for improving the overall efficacy of PDT and PTT.

Next, we took a simple approach to prepare NcPB into a nano agent. The solution of dimethyl sulfoxide (DMSO) involving NcPB was added to phosphate buffered saline (PBS) solutions containing Cremophor EL (CEL) in different volume percentages. As shown in Fig. 3a, in PBS solutions containing 0% CEL, the hydrodynamic diameter of NcPB was 122.6 nm and its polydispersity index (PDI) was 22.4%. A consistent result was also obtained in the transmission electron microscopy (TEM) detection. However, the NcPB in PBS solutions containing CEL contents of 0.1% and 0.5% was observed to be inhomogeneous from the dynamic light scattering (DLS) assay (Fig. S5a in Supporting information). When the content of CEL was increased to 1%, it showed a homogeneous dispersion system of NcPB with a PDI of 15.1% and an ultra-small nano-size of 12.3 nm, which is consistent with TEM imaging results (Fig. 3a).

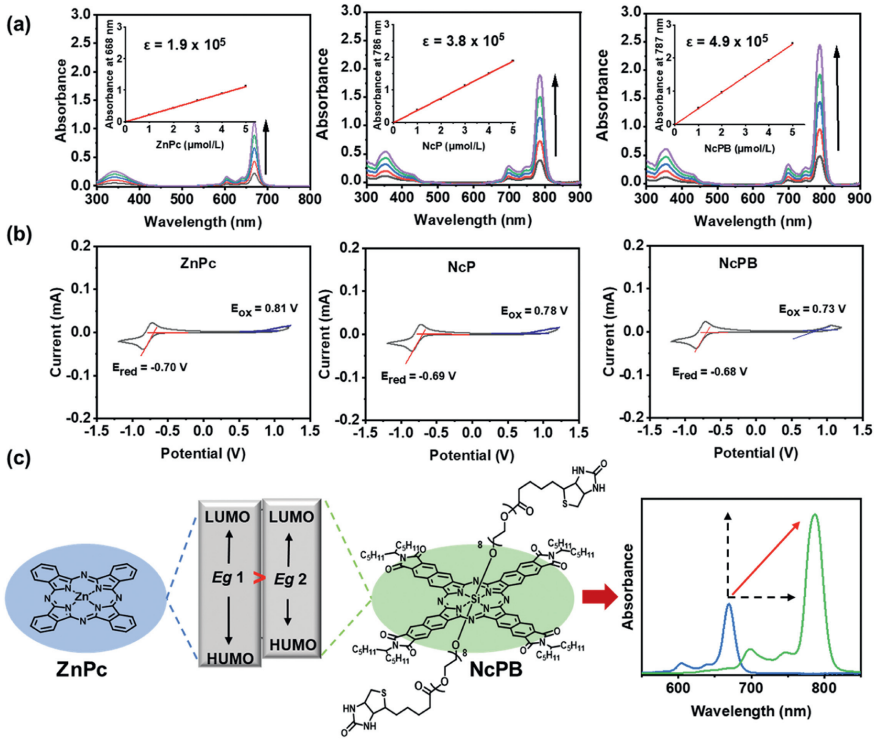

Fig. 2. (a) Electronic absorption spectra of ZnPc (left), NcP (middle) and NcPB (right) at different concentrations. The inset shows that the molar absorption coefficient is in accordance with Lambert's law. (b) Cyclic voltammogram of ZnPc (left), NcP (middle) and NcPB (right) in DMF using 0.1 mol/L $(n\text{-Bu})_4N^+PF^{6-}$ as a supporting electrolyte. Glassy carbon served as the working electrode, Ag/AgCl as a reference electrode, and Pt wire as the counter electrode. The scan rate was 100 mW/s. (c) Schematic representation of the difference in absorption wavelengths and light absorption capacities of ZnPc and NcPB.

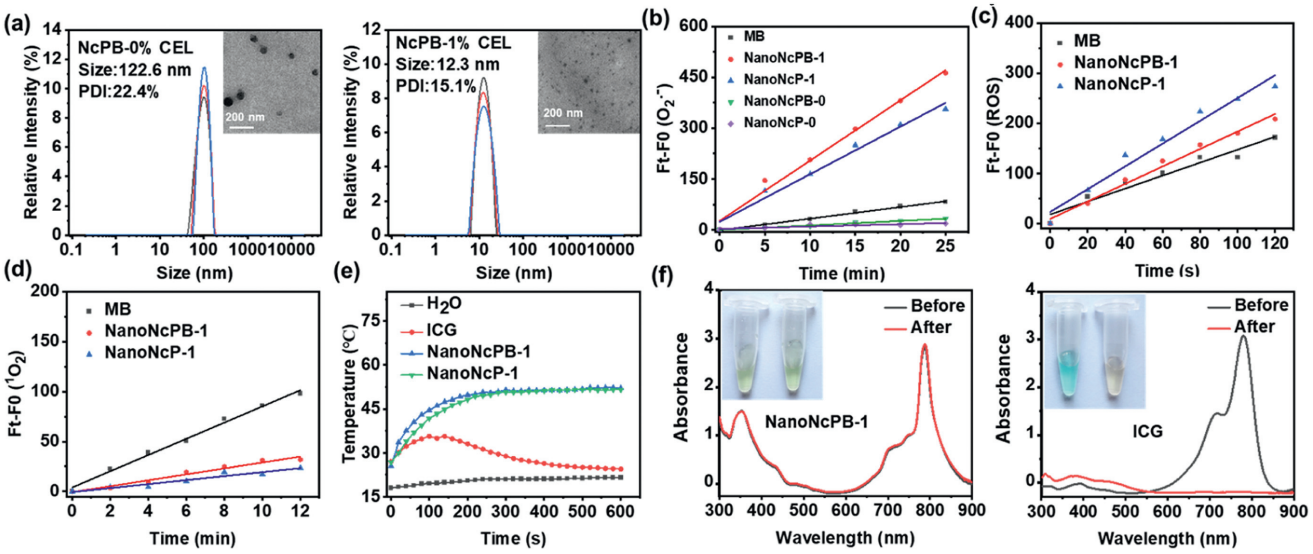

Fig. 3. (a) DLS assay of NcPB in PBS solutions without CEL (left) and PBS solutions containing 1% CEL (right). The inset shows the TEM assay. (b) DHE was utilized as the fluorescent probe to detect $O_2^{\bullet-}$ generation of MB and NanoNcPB-1 under light irradiation. (c) DCFH was used as the fluorescent probe to detect ROS generation of MB and NanoNcPB-1 under light irradiation. (d) SOSG was utilized as the fluorescent probe to detect $^1O_2$ generation of MB and NanoNcPB-1 under light irradiation. Light condition: $\lambda \geq 610$ nm, 1 mW/cm^2. (e) Temperature variations over time of ICG, NanoNcPB-1 and NanoNcP-1 (all at 20 μmol/L) in PBS solutions using the 785 nm laser irradiation for 10 min at a power density of 0.5 W/cm^2. (f) Electronic absorption spectra of NanoNcPB-1 (left) and ICG (right) before and after 10 min of 785 nm laser irradiation (0.5 W/cm^2). The inset displays pictures of NanoNcPB-1 and ICG before (left) and after (right) laser irradiation.

In addition, NcPB in PBS solutions containing 1% CEL showed no significant alteration in particle size over seven days (Fig. S5b in Supporting information). Moreover, we also performed the same method on NcP and used it as a control. The results show that NcP fails to form a nanosystem with uniform particle size in PBS solutions regardless of the adjustment of the CEL content (Fig. S6 in Supporting information). Here, we refer to the nanoparticles formed by assembled NcPB and NcP in PBS solutions without CEL as the NanoNcPB-0 and NanoNcP-0, respectively. Meanwhile, we refer to the nanoparticles formed by assembled NcPB and NcP in PBS solutions containing 1% CEL as the NanoNcPB-1 and NanoNcP-1, respectively.

The above studies show that NanoNcPB-0 and NanoNcPB-1 have different sizes. Herein, we separately studied the absorption spec-

tra of NanoNcPB-0, NanoNcPB-1 in PBS solutions, and NcPB in DMF. As shown in Fig. S7a (Supporting information), NcPB in DMF has a sharp and narrow Q-band absorption peak, while NanoNcPB-0 in PBS has a broad and low Q-band absorption peak. Interestingly, the light absorption capacity of NanoNcPB-1 is weaker than that of NcPB and stronger than that of NanoNcPB-0. In addition, the fluorescence emission intensity of NanoNcPB-1 is also between that of NcPB and NanoNcPB-0 (Fig. S7b in Supporting information). The electronic absorption and fluorescence emission spectra of NanoNcP-1 without the biotin unit are similar to those of NanoNcPB-1. We then investigated the ability of NanoNcPB-0, NanoNcP-0, NanoNcPB-1 and NanoNcP-1 to produce $O_2^{\bullet-}$ using the dihydroethidium (DHE) probe. As shown in Fig. 3b and Fig. S8 (Supporting information), both NanoNcPB-1 and NanoNcP-1 were able to produce higher amounts of $O_2^{\bullet-}$ and were 10-fold and 8-fold to commercial methylene blue (MB), respectively. However, both NanoNcPB-0 and NanoNcP-0 were less capable of producing $O_2^{\bullet-}$ than MB. Therefore, NanoNcPB-1 and NanoNcP-1with ultra-small particle size is more suitable than NanoNcPB-0 and NanoNcP-0 for type-I photoreaction. In addition, we also examined the ROS and $^1O_2$ production of NanoNcPB-1 and NanoNcP-1 using the 2,7-dichlorodi-hydrofluorescein diacetate (DCFH) and singlet oxygen sensor green (SOSG) probes, independently. The results showed that both NanoNcPB-1 and NanoNcP-1 were able to produce more ROS than MB (Fig. 3c and Fig. S9a in Supporting information). However, both of them produce little $^1O_2$ (Fig. 3d and Fig. S9b in Supporting information). These results suggested that NanoNcPB-1 and NanoNcP-1 should exert their photodynamic effects mainly through the type I pathway.

Besides, the photothermal conditions of NanoNcPB-1 and NanoNcP-1 have been investigated. As shown in Fig. 3e, compared to the commercially available photothermal agent indocyanine green (ICG), NanoNcPB-1 has a higher photothermal generation capacity, with temperature rising up to 52.5 °C under the 785 nm laser irradiation at a power density of 0.5 W/cm^2. In addition, the temperature of NanoNcP-1 is also consistent with that of NanoNcPB-1. Notably, the temperature of ICG showed a tendency to increase and then decrease when under continuous laser irradiation for 10 min, whereas the temperature of NanoNcPB-1 increased and then remained stable. This may be caused by the better photostability of NanoNcPB-1 than ICG. Therefore, the PBS solutions of ICG and NanoNcPB-1 after a continuous laser irradiation for 10 min were subjected to investigate the electronic absorption spectra. As shown in Fig. 3f, the absorbance of ICG decreased significantly after laser irradiation, whereas the absorbance of NanoNcPB-1 remained consistent with that before laser irradiation. This result indicates that NanoNcPB-1 has a better photothermal stability than ICG. Moreover, the photothermal cycling concurrently proved that NanoNcPB-1 can be stabilized in PBS solutions under a sustained laser irradiation for 80 min (Fig. S10a in Supporting information). We then studied the photothermal performances of NanoNcPB-1 at different concentrations and different light power densities. The results showed a more pronounced increase in temperature with increasing concentrations of NanoNcPB-1 (Fig. S10b in Supporting information). When the concentration of NanoNcPB-1 was 40 μmol/L, the temperature could rise to 58.0 °C under a laser irradiation at a power density of 0.5 W/cm^2. Moreover, the photothermal capacity of NanoNcPB-1 also increased with increasing laser power density. NanoNcPB-1 (20 μmol/L) showed no significant increase in temperature when exposed to a laser power density of 0.1 W/cm^2, whereas the temperature could increase up to 52.3 and 63.8 °C when exposed to a laser power density of 0.5 and 1.0 W/cm^2, respectively (Fig. S10c in Supporting information). These results suggest that NanoNcPB-1 should exerts photodynamic effects under a 785 nm laser irradiation at a power density equal to or less than 0.1 W/cm^2, whereas it may perform combined photothermal and photodynamic effects at a power density equal to or greater than 0.5 W/cm^2.

According to the aforementioned results, NanoNcPB-1 and NanoNcP-1 show superior photodynamic and photothermal characteristics, which have considerable potential for combination therapy of hypoxic tumor. Next, we proceeded to study the tumor targeting and phototherapy outcome of NanoNcPB-1 by building the subcutaneous hepatocarcinoma (H22) tumor-bearing mice. All animal studies were carried out in compliance with guidelines of the Animal Ethics Committee of Fuzhou University (No. 2023-SG-001), and also approved by the committee. Firstly, the *in vivo* biodistribution of NanoNcPB-1 was investigated by fluorescence imaging, and NanoNcP-1 was used as a control. As shown in Fig. 4a, at 36 h after intravenous injection, NanoNcPB-1 was significantly enriched in the tumor area. In contrast, NanoNcP-1 was rarely concentrated in the tumor tissues. Consequently, the fluorescence intensity of NanoNcPB-1 was 2.8-fold higher than that of NanoNcP-1 (Fig. 4b). In addition, to further validate that NanoNcPB-1 has the ability to actively select tumor tissues, we also constructed H22 tumor model at different locations in the trunk of ICR mice. The result showed that NanoNcPB-1 intelligently selects H22 tumor regardless of whether the tumor tissues are in the upper or lower trunk of the mouse (Fig. 4a). Secondly, an evaluation of the distribution of NanoNcPB-1 and NanoNcP-1 in the resected tumor and primary organs was conducted by taking the *ex vivo* fluorescence images at 72 h after intravenous injection. The findings demonstrated that NanoNcPB-1 has a significant fluorescent signal in the resected tumor tissues compared to NanoNcP-1 (Fig. 4c). Additionally, NanoNcPB-1 was taken up more in tumor tissues than in normal tissues, and its fluorescence signal in the tumor tissue was 6.1-fold higher than in liver and 4.7-fold more than in kidney (Fig. 4d).

In addition, we explored the potential of NanoNcPB-1 as a photothermal therapeutic agent and used PBS-injected mice as a control. Tumor tissues were irradiated by 785 nm laser with different power densities for 8 min at 36 h after intravenous injection of NanoNcPB-1, and temperature profiles of the tumor were observed using an infrared thermal imager. As shown in Figs. 4e and f, under laser irradiation at a power density of 0.1 W/cm^2, there was no significant temperature trend in both the NanoNcPB-1 and PBS groups. Notably, under the irradiation of a 785 laser with a power density of 0.5 W/cm^2, the temperature of the tumor tissues of mice injected with NanoNcPB-1 was significantly increased, rising to 58.0 °C. However, it was negligible temperature change of PBS-injected mice at a power density of 0.5 W/cm^2. Therefore, it is demonstrated that NanoNcPB-1 should perform both photodynamic and photothermal roles under NIR laser illumination at a power density of 0.5 W/cm^2.

The remarkable tumor accumulation capacity of NanoNcPB-1 inspired us to investigate its *in vivo* phototherapeutic efficacy in mice bearing H22 tumor. Six groups of mice (five mice each) were created: (1) handled with PBS in absence of laser irradiation (marked as PBS), (2) handled with PBS combined with 0.5 W/cm^2 laser irradiation (marked as PBS + 0.5 W/cm^2), (3) handled with PBS combined with 0.1 W/cm^2 laser irradiation (marked as PBS + 0.1 W/cm^2), (4) handled with NanoNcPB-1 in absence of laser irradiation (marked as NanoNcPB-1), (5) handled with NanoNcPB-1 combined with 0.5 W/cm^2 laser irradiation (marked as NanoNcPB-1 + 0.5 W/cm^2), and (6) handled with NanoNcPB-1 combined with 0.1 W/cm^2 laser irradiation (marked as NanoNcPB-1 + 0.1 W/cm^2). Following various treatments, the body weight and tumor volume of each mouse group were assessed every other day. Throughout the course of the treatments, the mice's body weights increased steadily and did not significantly differ between different groups (Fig. 4g). Nonetheless, there was a noticeable difference in the tumor volumes of the mice amongst the

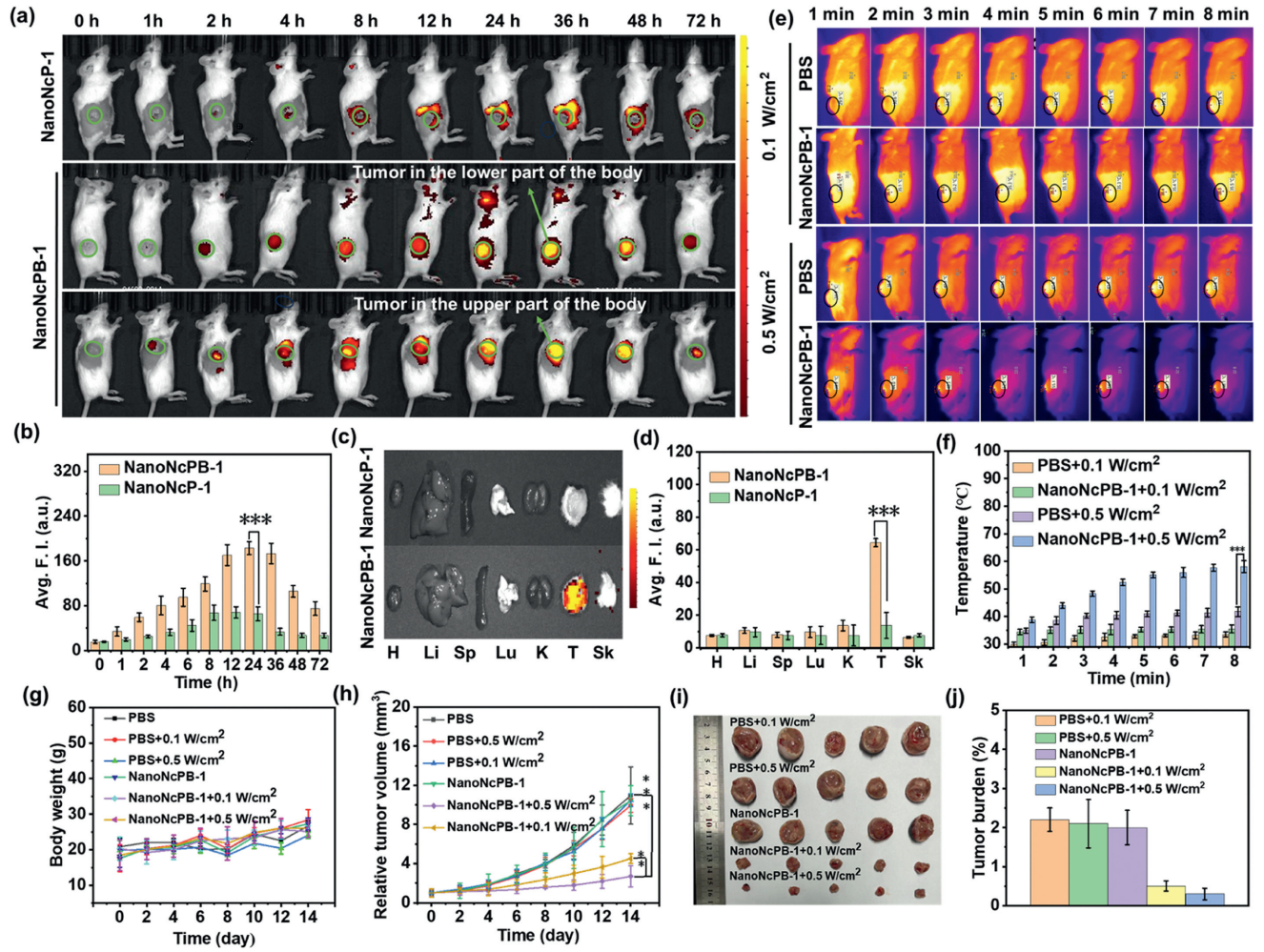

Fig. 4. (a) Typical fluorescence images of mice with H22 tumor before and after receiving an intravenous injection of NanoNcP-1 or NanoNcPB-1 (excited at 710 nm and received at 800 nm) at various intervals. (b) Analyzing the fluorescence signal intensities at the tumor site in mice that received an intravenous injection of NanoNcP-1 or NanoNcPB-1 (dose: 200 μmol/L 100 μL) at various intervals ($n = 5$). (c) *Ex vivo* fluorescence images of H22 tumor-bearing mice after receiving an intravenous injection of NanoNcP-1 or NanoNcPB-1. (d) Fluorescence intensities of various organs and tumor tissues in mice with H22 tumor were quantified following intravenous injection of NanoNcP-1 or NanoNcPB-1 ($n = 5$). H, heart; Li, liver; Sp, spleen; Lu, lung; K, kidney; T, tumor; Sk, skin; Avg. F. I., average fluorescence intensity. (e) *In vivo* photothermal imaging of mice with H22 tumor at 36 h after intravenous injection of NanoNcPB-1 under varying power levels of the 785 nm laser irradiation for 8 min. The control group consisted of mice injected with PBS. (f) Analyzing the photothermal signal of mice received an intravenous injection under varying power levels of the 785 nm laser irradiation ($n = 3$). (g) Average body weight changes of mice receiving the indicated treatments ($n = 5$). (h) Growth curve for tumor in H22-bearing mice following different treatments ($n = 5$). Light condition:785 nm laser, 0.1 or 0.5 W/cm^2, irradiation for 8 min. (i) Representative photos of isolated tumor in mice at 14 days after different treatments ($n = 5$). (j) Average tumor weights of mice after different treatments ($n = 5$). Data were expressed as mean ± SD. $^{**}P < 0.01$, $^{***}P < 0.001$. Analyzed using Student's *t*-test.

various groups. As shown in Fig. 4h, all of the control groups (PBS, PBS + 0.5 W/cm^2, PBS + 0.1 W/cm^2, and NanoNcPB-1) have a clear level of tumor growth, while the groups of NanoNcPB-1 + 0.1 W/cm^2 and NanoNcPB-1 + 0.5 W/cm^2 showed a significant inhibition of tumor growth. After 14 days of treatment, NanoNcPB-1 + 0.1 W/cm^2-treated mice's tumors showed 65% growth suppression, which should owe to the type-I PDT effect. The tumor inhibition of the NanoNcPB-1 + 0.5 W/cm^2 group was higher (92%) than that of the NanoNcPB-1 + 0.1 W/cm^2 group, indicating that the combination of type-I PDT and PTT should be advantageous. The exceptional antitumor efficaciousness of NanoNcPB-1 under laser irradiation was further validated by the representative images (Fig. 4i) and average tumor weights (Fig. 4j). In addition, pathological examination by the H&E staining was performed to evaluate the biological safety of NanoNcPB-1 on primary organs. It indicated that no obvious histopathological abnormality was observed from normal organs, verifying the excellent biocompatibility of NanoNcPB-1 (Fig. S11 in Supporting information).

Finally, we further studied the excretion of NanoNcPB-1 in the mouse body using a small animal *in vivo* fluorescence imager (Fig. S12 in Supporting information). As shown in Fig. S12a, at 24 h after intravenous injection, supine mice showed a visible fluorescent signal in the bladder, indicating that NanoNcPB-1 can be urinated out of the body. At the same time, we also monitored the fluorescence signals in urine and feces of mice over a period of 72 h (Fig. S12b). It was found that the fluorescence intensity of urine from mice was strongest at 24 h, while the signal at 72 h was negligible (Fig. S12c) in Supporting information, which is consistent with the results of *in vivo* imaging in supine mice. Moreover, fluorescent signal was also detected in mouse feces, but it was weaker than that in the urine of mice. Meanwhile, the urine is sent for high-resolution mass spectrometry to study the excretion product (Fig. S13 in Supporting information). It was found that the molecular ion peak of naphthalocyanine could be detected in urine. The result indicates that NanoNcPB-1 is excreted from the urine *via* the kidney in the original molecular manner. Next, we

also performed fluorescence imaging of isolated organs and tumor at 24 and 72 h after injection, respectively (Fig. S12d). As shown in Fig. S12e, both the dissected kidney and tumor had significant fluorescent signals at 24 h, whereas there were no signals in the heart, liver, spleen and lung. Notably, the fluorescent signal in the kidney disappeared at 72 h and remained evident only in the tumor tissues. Taken together, NanoNcPB-1 was effectively cleared by the kidneys and subsequently excreted through urine. This efficient clearance mechanism helps prevent the prolonged accumulation of nanoparticles in the body, contributing to the overall safety of their *in vivo* applications. Eventually, we also performed fluorescence imaging of blood at different time after intravenous injection of NanoNcPB-1 (Fig. S12f). It can undergo rapid *in vivo* blood circulation, resulting in a strong fluorescent signal at 2 h. However, the fluorescence signal in the blood gradually decreases as time goes on, and it disappears until 72 h (Fig. S12g). This result also provides further evidence that NanoNcPB-1 avoids the prolonged retention in the body of mice. In conclusion, NanoNcPB-1 is a renally removable PS that can be efficiently and rapidly excreted from the body.

In conclusion, a naphthalocyanine PS (NcPB) with an excellent NIR absorption was achieved by a molecular design strategy of extended conjugated units. Meanwhile, NcPB was formed into nanoparticle with an ultra-small size (NanoNcPB-1) through a supramolecular modulation strategy, which exhibited an effective type-I photoreaction and thermal generation, making it suitable for phototherapy of hypoxic tumor. As a result, assays reveal that NanoNcPB-1 shows an efficient accumulation to the tumor tissues and has a significant inhibition on solid tumor under the combined treatment of PDT and PTT. More importantly, this agent is rapidly excreted from mice as original medication *via* the renal clearance pathway, which avoids prolonged retention of PS in the body's circulation. Therefore, this NIR naphthalocyanine PS with outstanding light absorption, active targeting and renal clearance will encourage the continued exploration of clinical agents for phototherapy.

Declaration of competing interest

The authors declare that they have no known competing financial interests or personal relationships that could have appeared to influence the work reported in this paper.

CRediT authorship contribution statement

Li Li: Writing – original draft, Resources, Project administration, Methodology. **Jiale Wen:** Formal analysis. **Xiaojun Zhang:** Investigation. **Shuwen Fu:** Methodology. **Zixuan Chen:** Resources. **Kai Huang:** Software. **Luyue Fang:** Supervision. **Tinghe Zhao:** Validation. **Peipei Zhang:** Data curation. **Xingshu Li:** Writing – review & editing, Funding acquisition.

Acknowledgment

The authors thank the National Natural Science Foundation of China (Nos. T2322004 and 22078066).

Supplementary materials

Supplementary material associated with this article can be found, in the online version, at doi:10.1016/j.cclet.2024.110290.

References

[1] A. Mamun, Ann. Oncol. 30 (2019) vi138.
[2] S.E. Scott, C. Gildea, B.D. Nicholson, et al., Lancet Oncol. 24 (2023) 1242–1251.
[3] Y. Zhang, Y. Jiao, X. jia, et al., Chin. Chem. Lett. 35 (2024) 108748.
[4] L. Xu, J. Liu, J. Xi, et al., Small 14 (2018) 1800785.
[5] L. Wang, A. Mei, N. Li, et al., Chin. Chem. Lett. 35 (2024) 108974.
[6] J. Li, Y. Zhou, J. Liu, et al., J. Control. Release 352 (2022) 313–327.
[7] B. Zhang, L. Lin, J. Mao, et al., Chin. Chem. Lett. 34 (2023) 108518.
[8] D.J. Pinato, A. D'alessio, C. Celsa, G.F. Manfredi, C.A.M. Fulgenzi, Lancet 402 (2023) 1108–1110.
[9] W. Xu, D. Li, C. Chen, et al., Adv. Funct. Mater. 33 (2023) 2302231.
[10] Y. Dong, Y. Zou, X. Jia, et al., Smart Mol. 1 (2023) e20230001.
[11] X. Hu, Z. Fang, F. Sun, et al., Angew. Chem. Int. Ed. 63 (2024) e202401036.
[12] J. Guo, Y. Lin, S. He, et al., Chin. Chem. Lett. 35 (2024) 109537.
[13] V.N. Nguyen, S. Qi, S. Kim, et al., J. Am. Chem. Soc. 141 (2019) 16243–16248.
[14] H. Gu, W. Sun, J. Du, J. Fan, X. Peng, Smart Mol. 2 (2024) e20230014.
[15] Y.Y. Zhao, L. Zhang, Z. Chen, et al., J. Am. Chem. Soc. 143 (2021) 13980–13989.
[16] J. An, S. Tang, G. Hong, et al., Nat. Commun. 13 (2022) 2225.
[17] S.Y. Wang, Y.H. Pan, Y.C. Qu, et al., Smart Mol. 2 (2024) e20230024.
[18] C. Li, J. Ye, X. Yang, et al., ACS Nano 16 (2022) 18143–18156.
[19] Q. Yao, J. Fan, S. Long, et al., Chem 8 (2022) 197–209.
[20] Q. Li, A. Wang, J. Li, et al., Matter 5 (2022) 2425–2428.
[21] L. Li, J. Fu, J. Ye, et al., Adv. Mater. 21 (2024) 2310875.
[22] Y. Shao, B. Liu, Z. Di, et al., J. Am. Chem. Soc. 142 (2020) 3939–3946.
[23] R. Chang, Q. Zou, L. Zhao, et al., Adv. Mater. 34 (2022) 2200139.
[24] L. Yu, Y. Xu, Z. Pu, et al., J. Am. Chem. Soc. 144 (2022) 11326–11337.
[25] R. Xing, Q. Zou, C. Yuan, et al., Adv. Mater. 31 (2019) 1900822.
[26] L.K.B. Tam, J.C.H. Chu, L. He, et al., J. Am. Chem. Soc. 145 (2023) 7361–7375.
[27] C. Wang, Y. Sun, S. Huang, et al., J. Am. Chem. Soc. 145 (2023) 13099–13113.
[28] D. Zhang, K.X. Teng, L. Zhao, L.Y. Niu, Q.Z. Yang, Adv. Mater. 35 (2023) 2206188.
[29] M. Russo, H. Janekova, D. Meier, M. Generali, P. Stacko, J. Am. Chem. Soc. 146 (2024) 8417–8424.
[30] C.Y. Tsang, Y. Zhang, Chem. Soc. Rev. 53 (2024) 2898–2931.
[31] J. Shen, J. Karges, K. Xiong, et al., Biomaterials 275 (2021) 120979.
[32] Y. Bai, J. Hua, J. Zhao, et al., Adv. Sci. 11 (2024) 2306375.
[33] X. Guo, W. Sheng, H. Pan, et al., Angew. Chem. Int. Ed. 136 (2024) e202319875.
[34] S. Song, Y. Zhao, M. Kangl, et al., Adv. Mater. 36 (2024) 2309748.
[35] Y. Kim, J. Choi, E.H. Kim, et al., Adv. Sci. 11 (2024) 2309917.
[36] W. Li, J. Guo, E.C. Hobson, et al., Angew. Chem. Int. Ed. 63 (2024) e202401921.
[37] B. Li, M. Zhao, J. Lin, P. Huang, X. Chen, Chem. Soc. Rev. 51 (2022) 7692–7714.
[38] Y. Lee, S. Lee, S. Jon, Adv. Sci. 5 (2018) 1800017.
[39] G.X. Jin, C.C. Han, H.R. Zhao, et al., ACS Mater. Lett. 6 (2023) 375–383.
[40] M. Kim, D. Vanderlaan, J. Lee, et al., Nano Lett. 23 (2023) 9257–9265.